High-Resolution Frequency Analysis by the Use of Derivatives of the Fourier Transform: Application to Fluorescence Quantum Beats

Hirohiko Kono*, Isao Kawata, and Nobuhiro Ohta†

Department of Chemistry, Graduate School of Science, Tohoku University, Sendai 980-8578

†Research Institute for Electronic Science, Hokkaido University, Sapporo 060-0812

(Received December 8, 1998)

The v th frequency derivative of the Fourier spectrum obtained by the use of t^v-windows is proposed with some applications to practical examples. Derivative power spectra have higher resolution and lower base lines than conventional spectra (e.g., $v = 0$), and are insensitive to the choice of the beginning of the acquisition duration. For extremely large v, the spectrum is not resolved well. The optimal value of v is determined so that the main body of the product of the window t^v and the signal is accommodated in the range where the *S/N* ratio is relatively high. This criterion is successfully applied to a signal generated from a known spectrum and to fluorescence quantum beats in pyrimidine at zero and nonzero magnetic fields.

The Fourier transform has been established with numerous applications in various areas of research.[1—4] Nowadays a very large class of computational problems or data manipulations falls under the category of "Fourier transform methods". There is no doubt that the development of the fast Fourier transform has widened the area of application.[5—7] Although the Fourier transform is a solid mathematical theory, the practical evaluation of the Fourier transform in analyzing experimental data is not straightforward. Techniques are introduced to improve signal-to-noise ratio, or to raise the level of spectral resolution.[8—11] Most commonly used ones are filter, window, apodization, and zero filling.

In this paper, we propose to use higher order frequency derivatives of the Fourier spectrum. In practice, as shown in Sect.I, the v th derivative spectrum is obtained by applying the t^v-window to the temporal signal. High-resolution frequency analyses can be performed by the use of derivative power spectra. A criterion to determine the optimal v is provided. In Sect.II, derivative spectra for a signal generated from a known spectrum are calculated. It is demonstrated that the sample frequencies and intensities are recovered well in derivative spectra. The method is applied to analyze fluorescence signals in pyrimidine at zero and nonzero magnetic fields. The effect of magnetic field on the mixing among a singlet and triplet rovibronic levels is discussed.

I. Derivative Spectra

We consider an interferometric signal $I(t)$ such as fluorescence quantum beats or free induction decays in NMR. Such a signal can be represented by a Fourier cosine series

$$I(t) = \sum_j \int_{-\infty}^{t} \mathrm{d}t_0 f_j(t_0) \cos[\omega_j t - \phi_j(t_0)] \exp[-\gamma_j(t - t_0)], \quad (1)$$

where ω_j are beat frequencies, γ_j are relaxation constants, and $f_j(t_0)$ and $\phi_j(t_0)$ denote the amplitude and the phase for the mode j, respectively. The variable t_0 is introduced to express the distribution of onset times of quantum beats. We assume that the excitation process has ended at $t = 0$, i.e., $f_j(t_0) = 0$ for $t_0 \geqq 0$. The signal after the excitation process can be written as

$$\begin{aligned} I(t) &= \sum_j \int_{-\infty}^{0} \mathrm{d}t_0 f_j(t_0) \cos[\omega_j t - \phi_j(t_0)] \exp[-\gamma_j(t - t_0)] \\ &= \sum_j [a_j \cos(\omega_j t) + b_j \sin(\omega_j t)] \exp(-\gamma_j t), \end{aligned} \quad (2)$$

where a_j and b_j are the integrated amplitudes for ω_j

$$a_j = \int_{-\infty}^{0} \mathrm{d}t_0 f_j(t_0) \exp(\gamma_j t_0) \cos \phi_j(t_0), \quad (3)$$

$$b_j = \int_{-\infty}^{0} \mathrm{d}t_0 f_j(t_0) \exp(\gamma_j t_0) \sin \phi_j(t_0). \quad (4)$$

The Fourier spectrum (the characteristic function) of $I(t)$ is given by

$$\Phi(\omega) = \int_0^{\infty} \mathrm{d}t \exp(-i\omega t) I(t). \quad (5)$$

The v th derivative spectrum can be defined as ($v = 0$ means the ordinary Fourier transform)

$$\begin{aligned} F(\omega;\, v) &= i^v \frac{\mathrm{d}^v}{\mathrm{d}\omega^v} \Phi(\omega) \\ &= \int_0^{\infty} \mathrm{d}t t^v \exp(-i\omega t) I(t) \\ &= F_{\mathrm{C}}(\omega;\, v) + i F_{\mathrm{S}}(\omega; v), \end{aligned} \quad (6)$$

where, for Eq. 2, the real and imaginary parts are expressed as

$$F_C(\omega;\, v)=\sum_j \frac{\Gamma(v+1)/2}{[(\omega\pm\omega_j)^2+\gamma_j^2]^{(v+1)/2}} \times\left\{a_j\cos\left[(v+1)\tan^{-1}\left(\frac{\omega\pm\omega_j}{\gamma_j}\right)\right] \pm b_j\sin\left[(v+1)\tan^{-1}\left(\frac{\omega\pm\omega_j}{\gamma_j}\right)\right]\right\}, \quad (7)$$

$$F_S(\omega;\, v)=\sum_j \frac{\Gamma(v+1)/2}{[(\omega\pm\omega_j)^2+\gamma_j^2]^{(v+1)/2}} \times\left\{a_j\sin\left[(v+1)\tan^{-1}\left(\frac{\omega\pm\omega_j}{\gamma_j}\right)\right] \mp b_j\cos\left[(v+1)\tan^{-1}\left(\frac{\omega\pm\omega_j}{\gamma_j}\right)\right]\right\}. \quad (8)$$

The terms $\cos[(v+1)\tan^{-1}(\cdots)]$ are of absorptionlike type (= 1 at $\omega=\pm\omega_j$) and $\sin[(v+1)\tan^{-1}(\cdots)]$ are of dispersionlike type(= 0 at $\omega=\pm\omega_j$). For $v\geq 1$, the integrated intensity of $F(\omega;\, v)$ with respect to ω is zero (which reflects the fact that the signal $t^vI(t)$ is zero at $t=0$): the absorptionlike terms also have negative parts. Because of this, for $v\geq 1$, a positive definite spectrum cannot be obtained from any linear combination of F_C and F_S; that is, phase corrections are not meaningful.

The derivative spectra are, however, useful for deriving high-resolution power spectra. In many cases (e.g., for congested spectra), phase corrections are difficult to perform even for $v=0$: one must resort to the power spectrum. The v th power spectrum $P(\omega;\, v)$ can be defined as

$$P(\omega;\, v)\equiv|F(\omega;\, v)|^2 = F_C^2(\omega;\, v)+F_S^2(\omega;\, v). \quad (9)$$

Since the line shapes which peak in the domain of positive ω do not severely overlap with those in the negative domain, one can eliminate the interference terms between $\{\omega_j\}$ and $\{-\omega_k\}$:

$$P(\omega;\, v)\approx\sum_j\sum_k \frac{\Gamma(v+1)/2}{[(\omega\pm\omega_j)^2+\gamma_j^2]^{(v+1)/2}}\times\frac{\Gamma(v+1)/2}{[(\omega\pm\omega_k)^2+\gamma_k^2]^{(v+1)/2}} \times\left\{a_ja_k+b_jb_k+(a_jb_k-b_ja_k)\sin\left[(v+1)\times\left(\tan^{-1}\frac{\omega\pm\omega_k}{\gamma_k}-\tan^{-1}\frac{\omega\pm\omega_j}{\gamma_j}\right)\right]\right\}. \quad (10)$$

There remain interference terms between different modes j and k. As v becomes larger, the line shape functions $[(\omega\pm\omega_j)^2+\gamma_j^2]^{-(v+1)/2}$ become sharper: the interferences between different modes diminish. For $v>0$, we can therefore expect a desired sharp spectrum

$$P(\omega;\, v)\approx\sum_j \frac{(a_j^2+b_j^2)\Gamma^2(v+1)/4}{[(\omega\pm\omega_j)^2+\gamma_j^2]^{v+1}}. \quad (11)$$

Of course, there is a tradeoff, as usually required for any single window.[8,9] Our derivative spectrum which is equivalent to the use of the t^v window has undesired features. For extremely large v, the greater part of the signal intensity near the beginning of the acquisition duration (near $t=0$) is discarded. The power spectrum is then not resolved well; besides, the noise relatively enhanced near the end of the signal is amplified. The best value of v can be determined as follows. Suppose that a signal under consideration is multiplied by a window function $G(t)$ to reduce the noise level. Then, the envelope $S(t)$ of the data to be Fourier-transformed is

$$S(t)=t^vR(t)G(t), \quad (12)$$

where $R(t)$ is the smoothly varying envelope of the raw signal. For the v th derivative spectrum to be meaningful, the main body of $S(t)$ must be accommodated in the range where the *S/N* ratio is relatively high. We denote the end of such a time range by t_C. If $S(t)$ has a peak at t_P and a width t_W (both are functions of v), the requirement that v meets is equivalent to the inequality

$$t_P+t_W<t_C. \quad (13)$$

The largest v that satisfies Eq. 13 is the optimal value. If $R(t)=\exp(-\gamma t)$ and a Gaussian window $\exp(-t^2/\Delta t^2)$ is chosen as $G(t)$, t_P, and t_W are expressed as

$$t_P=\frac{\Delta t}{4}\left[-\gamma\Delta t+\sqrt{(\gamma\Delta t)^2+8v}\right], \quad (14)$$

and

$$t_W\approx t_P\Big/\sqrt{2(v+1)(t_P/\Delta t)^2+v\gamma t_P-v(v-1)}. \quad (15)$$

When one derives Eq. 15, a Poisson distribution is fitted to $S(t)$. Equation 15 is the standard deviation of the fitted Poisson distribution. In the next section, we apply the criterion Eq. 13 to obtain the best spectra for a signal generated from a known spectrum and for fluorescence quantum beats.

The quality of our window function t^v must be compared with those of other windows such as the sine-bell window. The sine-bell function $\sin[\pi t/t_f]$ is also zero at $t=0$ (t_f denotes the end of the acquisition duration) and usually provides a better spectrum than the ordinary $v=0$ Fourier transform without a window. However, the sine-bell power spectrum is not as sharp as the best derivative power spectrum of Eq. 9. The interference terms in the sine-bell spectrum are not expected to be as negligible as in Eq. 9. The exponential window $\exp(+\Gamma t)$ can also diminish the spectral width, but extremely amplifies the noise near the end of the signal. The parameter Γ needs to be chosen judiciously. In contrast to the exponential window, the t^v-window merely rises in proportion to the v th power of t.

II. Applications

A. A Test. A sample signal is prepared to check the ability of our derivative spectrum. We randomly generate 50 frequencies $\{\omega_j/2\pi\}$ between 0 and 50 MHz. The coefficients a_j and b_j are prepared according to a normal distribution with the mean value of 0. The frequencies and the intensities $a_j^2+b_j^2$ are shown in Fig. 1. The corresponding sample signal calculated from Eq. 2 is plotted in Fig. 2. The damping constants are set at $\gamma_j=3\times10^6$ s^{-1} for all j. The data are generated from 0 μs up to 4 μs at sampling intervals of 10 ns. Since no noise is superimposed, we here do not introduce any window other than t^v.

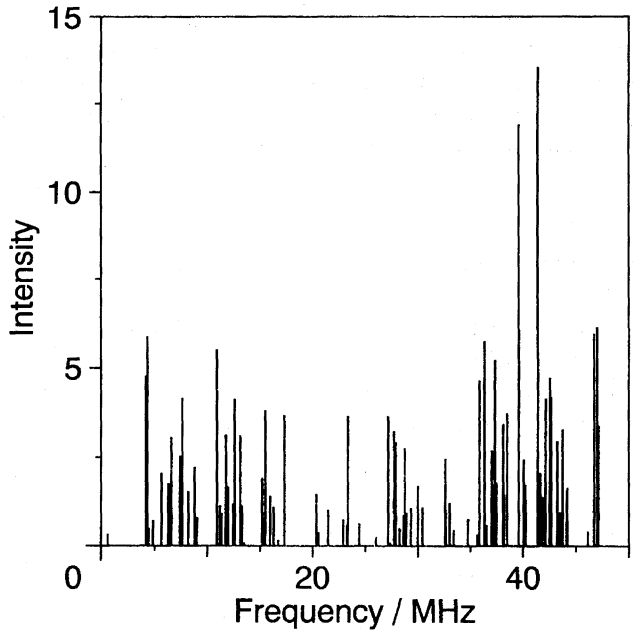

Fig. 1. Randomly generated 50 frequencies $\{\omega_j/2\pi\}$ between 0 and 50 MHz and their intensities $a_j^2+b_j^2$. The coefficients a_j and b_j are generated according to a normal distribution with the mean value of 0.

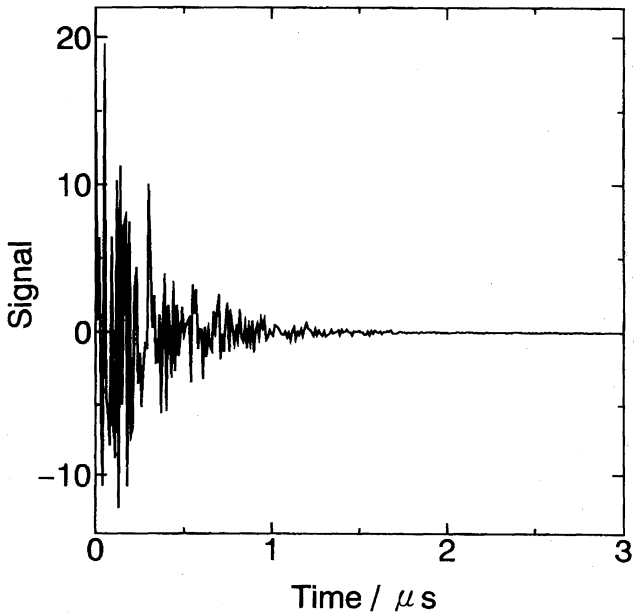

Fig. 2. A sample signal for the frequencies and intensities in Fig. 1. The damping constants are set at $\gamma_j = 3\times10^6\ s^{-1}$ for all j.

Figure 3 shows the derivative power spectra for $v = 0$, 1, 2, 4, 8, and 16. In comparison with Fig. 1, one finds in the ordinary Fourier spectrum ($v = 0$) that some peak intensities, such as those at 4 and 47 MHz, are strongly depressed. Apparently, derivative spectra are superior to the $v = 0$ spectrum. As the value v increases from 0 to 8, the resolution becomes higher; peaks in the spectrum become sharper or are split into fine peaks. The base line becomes lower, which indicates that the interferences between modes become weaker.

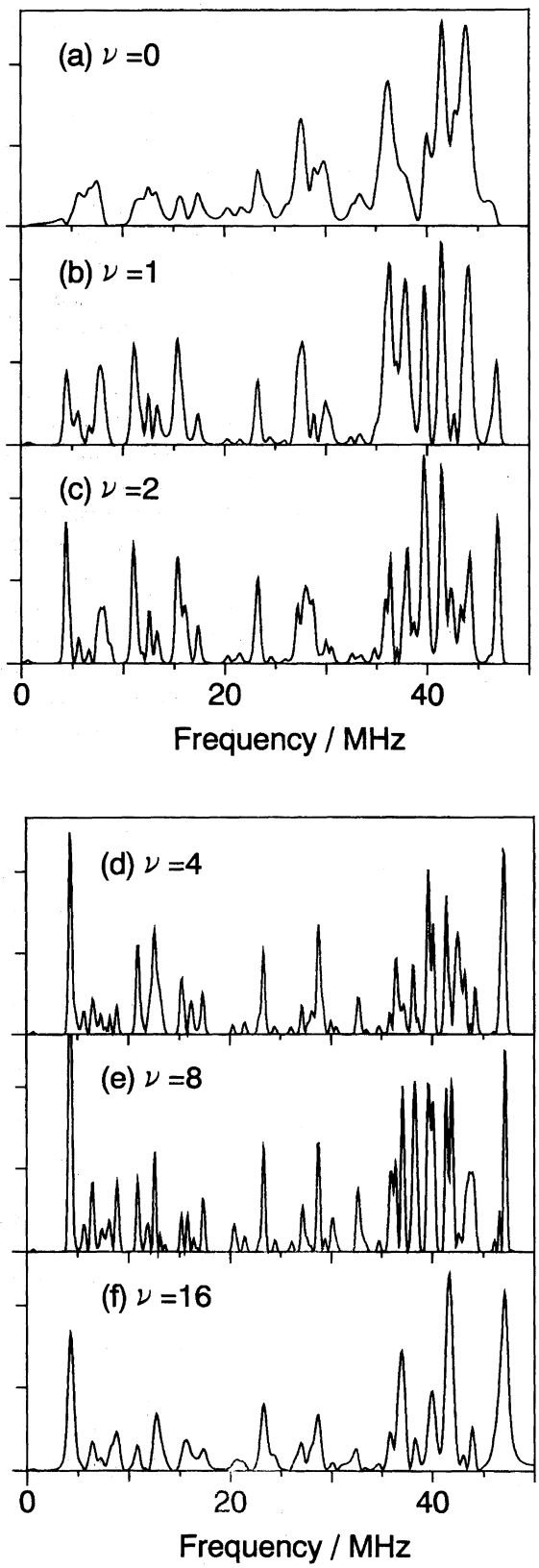

Fig. 3. Derivative power spectra for (a) $v = 0$; (b) $v = 1$; (c) $v = 2$; (d) $v = 4$; (e) $v = 8$, and (f) $v = 16$. The data shown in Fig. 2 is inputted. The end of the data acquisition duration is 4 μs.

The best spectrum is obtained for $v \approx 8$. As shown in Fig. 3e, most of the fine structures in Fig. 1 (with respect to the frequencies and intensities) are recovered. The resolution does not depend on the range of frequency.

For the present case, t_C in Eq. 13 is the end of the artificial data, 4 μs. Putting $\Delta t = \infty$ into Eqs. 14 and 15, we obtain $t_P = v/\gamma_j$ and $t_W = \sqrt{v}/\gamma_j$. Using the criterion Eq. 13, we find the optimal value $v = 8$, which is consistent with the conclusion drawn visually. For $v > 8$, most of the signal data in Fig. 2 are discarded by the window t^v; the resolution beomes lower. The quality of the spectrum begins to deteriorate as the v becomes larger than about 13. An example is shown in Fig. 3f.

The power spetrum for the sine-bell function is shown in Fig. 4. The spectrum is nearly identical with the derivative spectrum for $v = 1$. For the present signal, the first power of t in the sine-bell function plays the major role.

B. Analyses of Quantum Beats in Fluorescence. As a pratical example, we analyze time-resolved fluorescence signals (quantum beats) from the first excited singlet state S_1 in pyrimidine. It has been well known that in azaaromatic molecules such as pyrimidine fluorescence is quenched by an external magnetic field.[12—16] Fluorescence signals at zero and nonzero magnetic fields are analyzed in this subsection.

The experimental setup is as follows. Fluorescence decays of pyrimidine vapor were measured in a jet by using a digital memory (Iwatsu DM901). The excitation light source is a dye laser (Lambda Physik FL2002E) pumped by a XeCl excimer laser (Lambda Physik EMG 103MSC) equipped with KDP crystal and etalon. The linearly polarized UV light for excitation has a linewidth of ca. 0.1 cm^{-1} and a duration of ca. 10 ns. By employing the same apparatus and the same orthogonal geometry as mentioned in a previous paper,[13] the sum of the parallel and perpendicularly polarized components of fluorescence was monitored. An external magnetic field was applied with the direction perpendicular to the polarization direction of the excitation light, and fluorescence which proceeds along the same direction as the external field was observed. The data points were recorded at time intervals of 10 ns.

The optically prepared rovibronic level $|s\rangle$ in S_1 interacts with other dark levels $\{|\beta_j\rangle\}$ belonging to the other electronic states via intramolecular interaction (non-adiabatic coupling or spin-orbit coupling). In pyrimidine, spin-orbit coupling causes intersystem crossing (ISC) between the singlet and triplet electronic states, i.e., $\{|\beta_j\rangle\}$ are triplet rovibronic levels. The time evolution of $|s\rangle$, $|\Psi(t)\rangle$, can be written in terms of eigenstates $\{|n\rangle\}$ of the total Hamiltonian $\boldsymbol{H}$

$$|n\rangle = \alpha_n|s\rangle + \sum_j \beta_{nj}|\beta_j\rangle, \tag{16}$$

where the coefficients are to be determined by the energies of $|s\rangle$ and $\{|\beta_j\rangle\}$ and their coupling strengths.

If the pulse duration is shorter than $\hbar/\Delta E$, where ΔE is the absorption width over which the s-character is distributed, the initially prepared state is equivalent to the bright level $|s\rangle$. The time evolution is then given by

$$|\Psi(t)\rangle = \exp(-i\boldsymbol{H}t/\hbar)|s\rangle = \sum_n \alpha_n^*|n\rangle e^{-i\omega_n t}, \tag{17}$$

where ω_n are eigenvalues of $\boldsymbol{H}$. The fluorescence intensity $I_f(t)$ is proportional to $|\langle s|\Psi(t)\rangle|^2$

$$I_f(t) \propto \left\{ \sum_n |\alpha_n|^4 e^{-\gamma_n t} + 2\sum_{n<m}\sum |\alpha_n|^2|\alpha_m|^2 \times \cos[(\omega_n - \omega_m)t] e^{-(\gamma_n+\gamma_m)t/2} \right\}. \tag{18}$$

where γ_n is the longitudinal relaxation rate of the eigenstate $|n\rangle$. The first sum represents the population decays of individual eigenstates (incoherent sum) and the second one represents the interference among eigenstates (coherent sum). The observed fluorescence consists of signals with different onset times.

The fluorescence decay pattern depends on how many background levels are effectively coupled to the bright level $|s\rangle$. If the number of effectively coupled background levels, N_{eff}, is small, the coherent sum generates quantum beats. The Fourier analysis of the beat decay provides not only energy differences between eigenstates but also coupling strengths. For a review of quantum beat spectroscopy of molecules, the reader is referred to Ref. 17. On the other hand, when N_{eff} is large, the coherent sum generates a single fast exponential decay. In-between, a biexponential decay, which consists of the fast decay generated from the coherent sum and the slow exponential decay from the incoherent sum, can be observed. See Refs. 12, 13, 14, 15, and 16, for the details.

Fluorescence signals of pyrimidine at various magnetic field strengths H are analyzed by derivative power spectra. The excitation is tuned to the P(1) rotational line of the 12_0^2 vibrational band.

(i) At zero field: The fluorescence signal at zero field is plotted in Fig. 5. Quantum beats are superimposed in the slow exponential decay of $\gamma \approx 3\times10^6$ s^{-1}. For the analysis, the fluorescence signal counted during the excitation process is discarded (until 100 ns after the initial rise in Fig. 5) and about 900 data points (for ca. 9 μs) are used. The noise level is reduced by multiplying the data by a Gaussian window $\exp(-t^2/\Delta t^2)$. We chose $\Delta t = 0.7$ μs. The *S/N* ratio is still as high as 10^2 at $t = 0.7$ μs. The ordinary Fourier power spectrum ($v = 0$) is shown in Fig. 6a and the derivative power spectrum for $v = 2$ is shown in Fig. 6b.

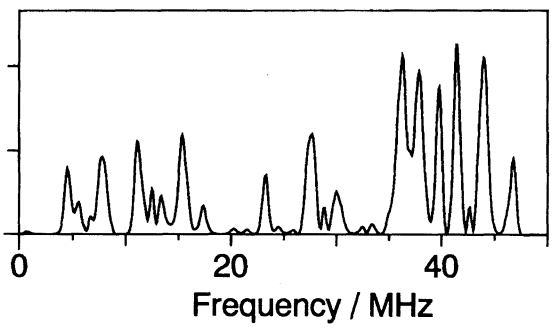

Fig. 4. The power spectrum for the sine-bell function. The signal used is the same as in Fig. 3.

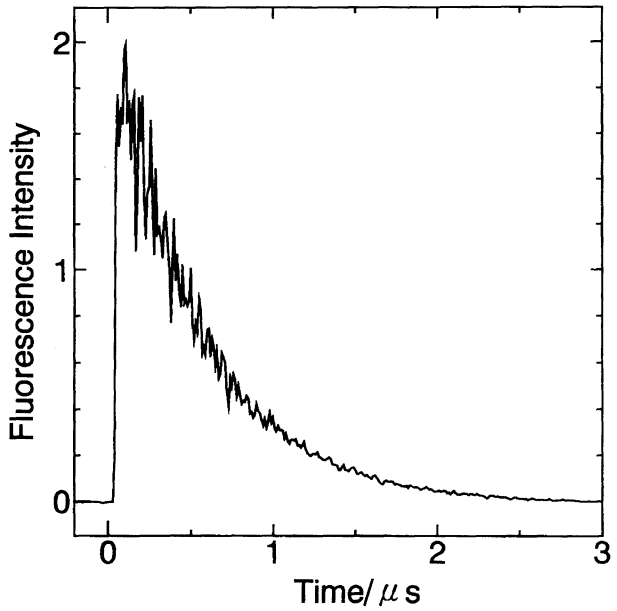

Fig. 5. The fluorescence signal at the P(1) excitation of 12_0^2 in pyrimidine (at $H = 0$ G). The data points are recorded at intervals of 10 ns.

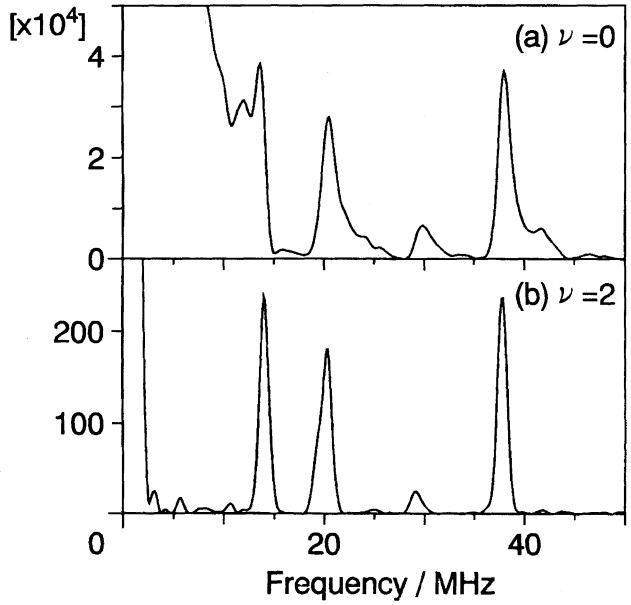

Fig. 6. Power spectra for the fluorescence signal in Fig. 5 : (a) $v = 0$; (b) $v = 2$. The fluorescence signal counted during the excitation process is discarded (until 100 ns after the initial rise in Fig. 5) and about 900 data points (≈ 9 μs) are used. The noise level of the signal is reduced by the Gaussian window of width $\Delta t = 0.7$ μs.

To severely estimate t_C in Eq. 13, t_C should be replaced with Δt. Putting Eqs. 14 and 15 into the criterion $t_P + t_W < \Delta t$, we find the optimal value $v = 2$. Evidently the peaks in Fig. 6b are much sharper than those in Fig. 6a. The base line in Fig. 6b is lower, as expected. The resolution in Fig. 6a is especially low at low frequencies because the ordinary Fourier transform cannot resolve the slowly decaying envelope in the signal. In contrast to it, in Fig. 6b, the dominant zero frequency component is narrowed: the resolution in the $v = 2$ case is satisfactory even in the low frequency range. It should be pointed out that the ambiguous procedure of eliminating the slowly decaying envelope (which is not uniquely defined) is avoided in obtaining the high resolution spectrum in Fig. 6b.

(ii) $H = 15$ G: The fluorescence signal at magnetic field strength $H = 15$ G is plotted in Fig. 7 (1 G = 10^{-4} T). In the spectral analysis shown in Fig. 8, the signal is multiplied by the Gaussian of width $\Delta t = 0.7$ μs. The overall feature of the signal looks like that in Fig. 5, but the amplitudes of beats are smaller. At zero field, the total angular momentum

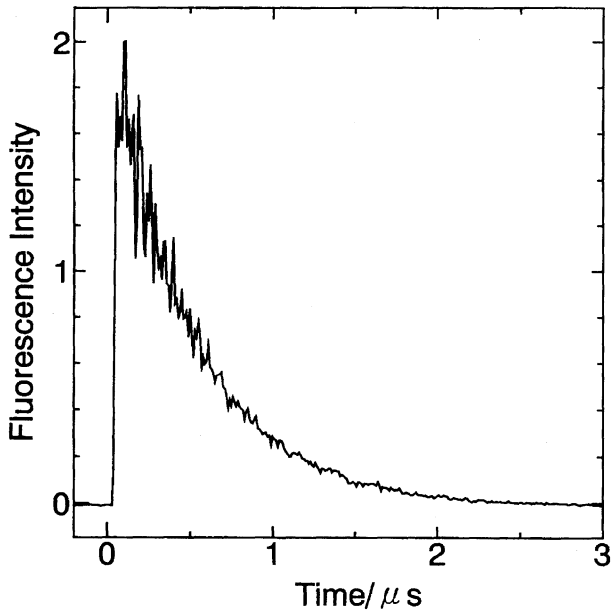

Fig. 7. The fluorescence signal at P(1) of 12_0^2 in pyrimidine at $H = 15$ G.

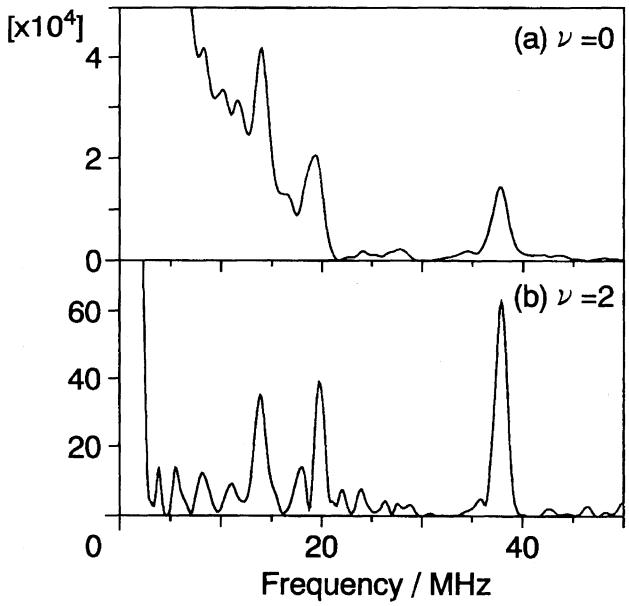

Fig. 8. Power spectra for the signal in Fig. 7: (a) $v = 0$; (b) $v = 2$. The original signal is treated with the same data manipulation as in Fig. 6.

J is conserved in ISC. When a magnetic field is applied, the triplet spin sublevels with different J are mingled among one another by the Zeeman interaction.[12,18—23] The singlet level can interact with all the spin sublevels mingled. In addition to level shifts, this causes an increase in N_{eff}.[12—16] More beat frequencies are expected to be involved in the fluorescence signal. Because of a random distribution of beat frequencies,[16] the beat amplitudes becomes smaller, as observed. Comparing the Fourier spectra of $v = 0$ in Figs. 6a and 8a, one finds that most of the peaks at zero field remain at 15 G and are shifted only a little.[24] These peaks are broadened by the magnetic field. For $v = 0$, the magnetic field effect is characterized by the broadening of the main peaks in the spectrum. For $v = 2$, as shown in Fig. 8b, new frequencies appear around the two main frequencies of 14 and 20 MHz. At $H = 15$ G the main peaks at zero field remain (the intensities of the main peaks are lowered). The $v = 2$ spectrum at 15 G is characterized by the appearance of new frequencies, instead of the broadening of peaks.

(iii) $H = 29$ G: The fluorescence signal at $H = 29$ G is plotted in Fig. 9 and the spectral analysis is shown in Fig. 10 ($\Delta t = 0.7$ μs is used). Most peaks in Fig. 10b are nearly on the same order in intensity, indicating that the absorption intensity of s-character is efficiently redistributed by the magnetic field. The two main peaks at 14 and 20 MHz observed at zero field collapse, as shown in Fig. 10b. As the field strength increases, these main peaks collapse.

The appearance of new frequencies and the collapse of the main peaks agree with the idea that a magnetic field increases N_{eff}. Most of the newly emerging frequencies are distributed around the main peaks observed at zero field. This is in accord with the proposed mechanism of the increase in N_{eff}.[16,25] The main peaks at zero field originate from the triplet levels $\{|u_j\rangle\}$ strongly coupled with the singlet level $|s\rangle$.

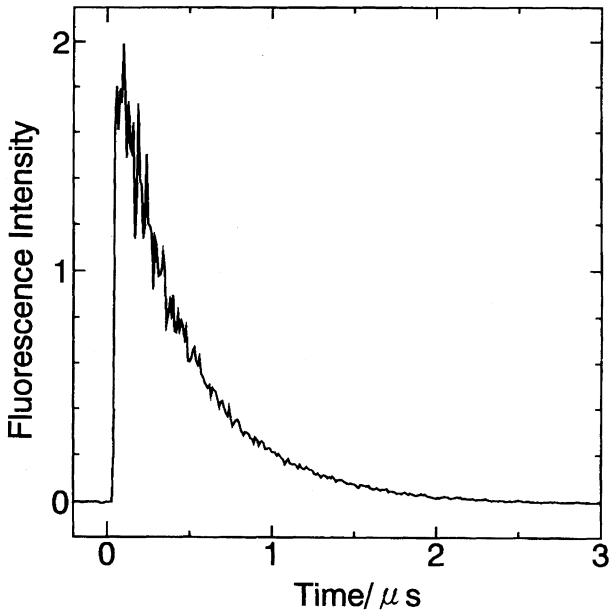

Fig. 9. The fluorescence signal at P(1) of 12_0^2 in pyrimidine at $H = 29$ G.

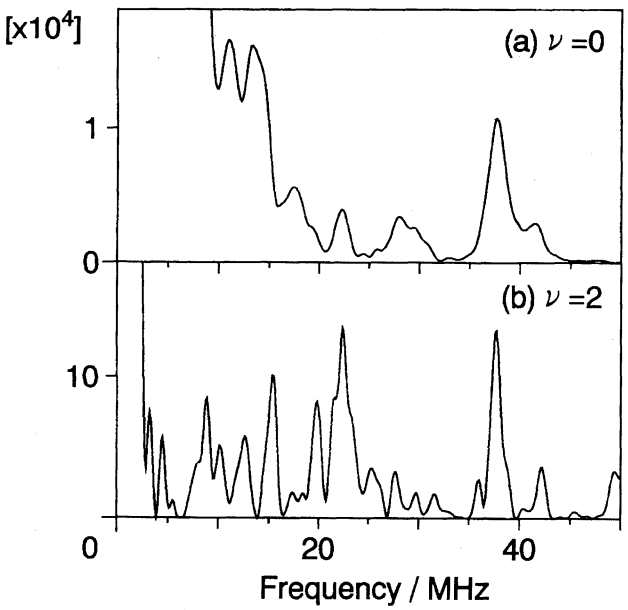

Fig. 10. Power spectra for the signal in Fig. 9: (a) $v = 0$; (b) $v = 2$. The original signal is treated with the same data manipulation as in Fig. 6.

It has been demonstrated[16,25] that at nonzero field strengths a triplet level $|v\rangle$ that is not coupled to $|s\rangle$ at zero field can strongly interact with nearby levels of $\{|u_j\rangle\}$. As a result, peaks of new frequencies are distributed around main peaks observed at zero field.

The derivative spectrum is very sensitive to the change in magnetic field strength. We believe that the derivative spectrum will be a very useful tool for identifying the locations of peaks and for detecting slight modifications in the signal.

III. Concluding Remarks

The derivative Fourier spectrum using t^v-windows is founded on the application to a sample signal and observed quantum beats. No awkward parameters are involved in the derivative spectrum. The resolutions of derivative power spectra are higher than the ordinary $v = 0$ Fourier power spectrum and the spectrum treated with the sine-bell function. The base line is lower than the $v = 0$ spectrum. Besides these advantages, the derivative spectra are insensitive to the choice of the beginning of the acquisition duration (the signal after this time is converted to the frequency domain), while the peak intensity and line shape for $v = 0$ are sensitive to it.

For extremely large v, the greater part of the signal intensity near the beginning of the acquisition duration is discarded and the noise relatively enhanced near the end of the signal is amplified. The power spectrum is then not resolved well and is dominated by the noise. The best value of v is determined by the criterion that the main body of the product of the t^v-window and the signal is accommodated in the range where the S/N ratio is relatively high. This criterion is successfully applied to a signal generated from a known spectrum (Sect.IIA) and to fluorescence quantum beats in pyrimidine (Sect.IIB). In Sect.IIA, the sample frequencies and intensities are well recovered by the derivative spectra

of $v \approx 8$. In Sect.IIB, fluorescence signals at zero and nonzero magnetic fields are analyzed using derivative spectra. It is found that the absorption intensity of singlet character is efficiently redistributed by a magnetic field. New frequencies are distributed around main peaks observed at zero field, which is in accord with the proposed mechanism of the increase in N_{eff}.[16,25] The derivative spectrum is very sensitive to the change in magnetic field strength and proves to be useful to detect slight modifications in the signal.

In conclusion, the t^v-window can serve as a practical tool to raise the level of resolution.

This work was supported in part by a Grant-in-Aid for Scientific Research No. 08640631 from the Ministry of Education, Science, Sports and Culture. One of the authors (H.K.) would like to thank Dr. K. Akiyama for helpful discussions.

References

1) D. C. Champeney, "Fourier Transforms in Physics," Hilger, Bristol (1985).

2) R. N. Bracewel, "The Fourier Transform and Its Applications," McGraw, New York (1986).

3) G. B. Folland, "Fourier Analysis and Its Applications," Wadsworth & Brooks, Pacific Grove (1992).

4) J. R. Higgins, "Sampling Theory in Fourier and Signal Analysis," Clarendon, Oxford (1996).

5) H. J. Nussbaumer, "Fast Fourier Transform and Convolution Algorithms," Springer, Berlin (1982).

6) E. O. Bringham, "The Fast Fourier Transform and Its Applications," Prentice, Englewood (1988).

7) C. van Loan, "Computational Frameworks for the Fast Fourier Transform," SIAM, Philadelphia (1992).

8) R. R. Ernst, G. Bodenhausen, and A. Wokaun, "Principles of Nuclear Magnetic Resonance in One and Two Dimensions," Clarendon, Oxford (1987).

9) P. A. Angelidis, *Concepts Magn. Reson.*, **8**, 339 (1996).

10) A. V. Oppenheim and R. W. Schafer, "Digital Signal Processing," Prentice, London (1975).

11) F. J. Harris, *Proc. IEEE*, **66**, 52 (1978).

12) See, for example: N. Ohta, *J. Phys. Chem.*, **100**, 7298 (1996).

13) N. Ohta and T. Takemura, *J. Chem. Phys.*, **95**, 7119 (1991).

14) A. Frad, F. Lahmani, A. Tramer, and C. Tric, *J. Chem. Phys.*, **60**, 4419 (1974); F. Lahmani, A. Tramer, and C. Tric, *J. Chem. Phys.*, **60**, 4431 (1974).

15) J. M. Delory and C. Tric, *Chem. Phys.*, **3**, 54 (1974).

16) H. Kono and N. Ohta, *J. Chem. Phys.*, **103**, 162 (1995).

17) E. Hack and J. R. Huber, *Int. Rev. Phys. Chem.*, **110**, 287 (1991); H. Bitto and J. R. Huber, *Acc. Chem. Res.*, **25**, 65 (1992).

18) M. Lombardi, "Excited States," ed by E. C. Lim, Academic, New York (1988), Vol. 7, p. 163.

19) W. E. Howard and E. W. Schlag, "Radiationless Transitions," ed by S. H. Lin, Academic, New York (1980), p. 81.

20) J. C. D. Brand, C. di Lauro, and D. S. Liu, *Can. J. Phys.*, **53**, 1853 (1975).

21) P. R. Stannard, *J. Chem. Phys.*, **68**, 3932 (1978).

22) A. Matsuzaki and S. Nagakura, *Helv. Chim. Acta*, **61**, 675 (1978).

23) N. Ochi and S. Tsuchiya, *Chem. Phys.*, **152**, 319 (1991).

24) The projection of the total angular momentum J onto the magnetic field axis, M_J, is conserved in ISC. For the P(1) excitation, the triplet levels interacting with the $J = 0$ singlet level have $M_J = 0$. In this case, the first order Zeeman energies of the triplet sublevels vanish. See, for example, Ref. 20. The level shifts are caused by the Zeeman interactions between spin sublevels. This type of second order shift is much smaller than the Larmor frequency $g\beta_B H$.

25) N. Ohta, I. Yamazaki, and H. Kono, *J. Phys. Chem.*, **101**, 452 (1997).